Hydrides of Alkaline Earth-Tetrel (AeTt) Zintl Phases: Covalent Tt-H Bonds from Silicon to Tin

Henry Auer,[†] Robin Guehne,[‡] Marko Bertmer,[‡] Sebastian Weber,[†] Patrick Wenderoth,[¶] Thomas Christian Hansen,[§] Jürgen Haase,[‡] and Holger Kohlmann[*,†]

[†]*Leipzig University, Department of Inorganic Chemistry, Johannisallee 29, 04103 Leipzig, Germany*

[‡]*Leipzig University, Department of Experimental Physics II, Linnéstraße 5, 04103 Leipzig, Germany*

[¶]*Saarland University, Department of Inorganic Solid-State Chemistry, Am Markt, Zeile 3, 66125 Saarbrücken, Germany*

[§]*Institut Laue-Langevin, 71 Avenue des Martyrs, CS 20156, 38042 Grenoble cedex 9, France*

E-mail: holger.kohlmann@uni-leipzig.de

Phone: +49 341/97-36201. Fax: +49 341/97-36199

1

Abstract

Zintl phases form hydrides either by incorporating hydride anions (interstitial hydrides) or by covalent bonding of hydrogen to the polyanion (polyanionic hydrides), which yields a variety of different compositions and bonding situations. Hydrides (deuterides) of SrGe, BaSi and BaSn were prepared by hydrogenation (deuteration) of the CrB-type Zintl phases AeTt and characterized by laboratory X-ray, synchrotron and neutron diffraction, NMR spectroscopy and quantum chemical calculations. $SrGeD_{4/3-x}$ and $BaSnD_{4/3-x}$ show condensed boat-like six-membered rings of Tt atoms, formed by joining three of the zig-zag chains contained in the Zintl phase. These new polyanionic motifs are terminated by covalently bound hydrogen atoms with d(Ge-D) = 1.521(9) Å and d(Sn-D) = 1.858(8) Å. Additional hydride anions are located in Ae_4 tetrahedra, thus both features of interstitial hydrides and of polyanionic hydrides are represented. $BaSiD_{2-x}$ retains the zig-zag Si-chain as in the parent Zintl phase, but in the hydride (deuteride) it is terminated by hydrogen (deuterium) atoms, thus forming a linear (SiD)-chain with d(Si-D) = 1.641(5) Å.

Introduction

Zintl phases are polar intermetallic compounds of a group one or two metal and a group 13 to 16 element. According to the Zintl-Klemm concept[1–7] the more electronegative element forms polyanionic partial structures that resemble features of the formally isoelectronic element structure, e.g., CrB-structure type Zintl phases AeTt, Ae = Ca-Ba, Tt = Si-Pb, form linear $_1^\infty[Tt^{2-}]$ zig-zag chains like in chalcogens.

The reactions of hydrogen with Zintl phases have only recently started to be explored systematically. According to Häussermann two general types of Zintl phase hydrides may be distinguished: (i) interstitial hydrides, where ionic hydride (H^-) is coordinated by the cationic framework exclusively and (ii) polyanionic hydrides, where hydrogen binds covalently to the Zintl polyanion.[8]

Gallium shows a rich chemistry of polyanionic hydrides that can be rationalized by an extended Zintl concept, e.g., it forms neopentane-like $(Ga[GaH_3]_4)^{5-}$,[9] propane-like $(Ga_3H_8)^{3-}$,[10] or polyethylene-like $([GaH_2]_n)^{n-}$ structures[9,11]. The Zintl phases $AeTr_2$, Ae = Sr, Ba, Tr = Al, Ga react with hydrogen (deuterium) to form $AeTr_2H_2$, which show hydrogen (deuterium) puckered Tr honeycomb layers (6^3 nets).[12–14] This can be rationalized since $(TrH)^-$ has the same valence electron configuration as polysilicon hydride $(SiH)_\infty$.

While Zintl phases containing group 13 elements show a strong trend in forming polyanionic hydrides, the existence of such motifs for group 14 elements is still under discussion. Covalent Si-H bonds could be shown for $ASiH_3$, A = K-Cs, but the tetrahedral Si_4^{4-} units of the parent phases ASi are broken up and we find isolated SiH_3^--groups.[15–18] The Zintl phase Ba_3Si_4 that shows distorted butterfly tetrahedral $(Si^{2-})_2(Si^-)_2$-polyanions behaves differently forming a interstitial hydride.[19] The mixed compounds AeTrTt, Ae = Ca-Ba, Tr = Al, Ga, (In), Tt = Si-Sn, that are electronically imbalanced Zintl phases, form electron precise polyanionic hydrides Ae(TrH)Tt, where hydrogen only binds to the group 13 element.[20–23]

Most promising candidates for polyanionic hydrides of group 14 are the phases derived from CrB-structure type Zintl phases. Early work by Ohba *et al.* claimed covalently bound hydrogen in $CaSiH_{1.3}$ next to hydride filled tetrahedral Ca_4-voids.[24] This was denied by Wu *et al.* relying on neutron vibrational spectroscopy as well as neutron diffraction data.[25] Since then a couple of similar hydride (deuteride) phases were described, e.g., $SrSiH_{1.6}$ and $BaSiH_{3.4}$,[26,27] as well as $NdGaH_{1.66}$[28] and $GdGaH_x$[29].

In this contribution we reinvestigate the barium compound and classify it as $BaSiH_{2-x}$. We also show the existence of two new hydride phases $SrGeH_{4/3-x}$ and $BaSnH_{4/3-x}$. SrSn does not show any reactivity towards hydrogen, while SrPb and BaPb decompose into $SrH_2 + SrPb_3$ and $BaH_2 + Ba_3Pb_5$. There are at least two additional hydrogen (deuterium) poor phases in the $SrGe-H_2$ system, which will be discussed in a forthcoming paper[30]. Therefore, as it is the hydrogen (deuterium) richest compound, $SrGeH_{4/3-x}$ will alternatively be called γ-$SrGeH_y$. A combination of diffraction methods (laboratory X-ray, synchrotron and neutron), solid-state

3

nuclear magnetic resonance spectroscopy as well as quantum chemical calculations strongly suggest a covalent bond between Si/Ge/Sn and hydrogen (deuterium) and therefore show the first examples for well established polyanionic hydrides of the tetrels.

Experimental Section

Synthesis

All manipulations were done in an argon filled glovebox. Oxygen and moisture content were both monitored and kept below 1 ppm.

BaSi was prepared from the elements (Si: ChemPur, 99.9999%; Ba rod: 99.3%) in an electric arc furnace. A 5% barium excess was used to compensate the evaporation of alkaline earth metal. Samples were remelted several times to improve homogeneity. SrGe was prepared from the elements (Ge: ChemPur, 99.9999%; Sr: ChemPur, 99%, under oil, washed in dry hexane) in welded niobium or tantalum jackets sealed in quartz ampules. The sample was melted at 1560 K and annealed at 1370 K for 48 h. As tin and lead react with the niobium or tantalum, for the other samples steel jackets were used. BaSn and SrSn were prepared from the elements (Sn powder: ChemPur, 99+%; Ba, Sr: as above). They were annealed at 1270 K for 48 h, then ground and annealed at 1270 K for 48 h again. BaPb and SrPb were prepared from the elements (Pb powder: Alfa Aesar, 99.95%; Ba, Sr: as above). They decompose peritectically and thus they were melted at 1270 K and quenched in cold water. Subsequently, SrPb was annealed at 970 K for 48 h and BaPb was annealed at 1010 K for 48 h.

Hydrides (H_2: Air Liquide, 99.9%) and deuterides (D_2: Air Liquide, 99.8% isotope purity) of BaSi, SrGe and BaSn were prepared using an autoclave made from hydrogen resistant Nicrofer® 5219Nb-alloy 718. Tab. 1 summarizes the hydrogenation conditions for the syntheses. The corresponding deuterides were prepared under the same conditions as the hydrides. The alkaline earth metal to tetrel ratio of the hydrides was confirmed by EDX.

Zintl phases as well as their hydrides are grey brittle powders. The hydrides easily cleave (Fig. 1) as described by Armbruster for $CaSiH_x$.[26,27] While the hydride of BaSi decomposes slowly in air, the hydrides of SrGe and BaSn rapidly react with moisture. The decomposition products of the hydrides are powders that are amorphous to X-ray diffraction. In the case of SrGe the color changes to yellow.
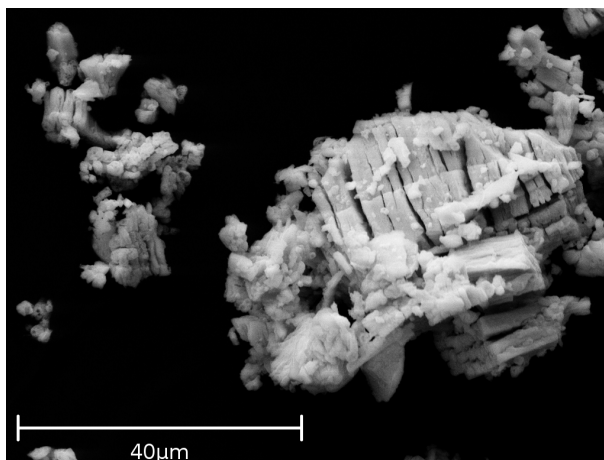

Figure 1: Scanning electron microscope (secondary electron detector) picture of $BaSnD_{4/3-x}$. The crystals are brittle and easily cleave to form plates.

Table 1: Hydrogenation conditions for Zintl phases AeTt, Ae = Sr, Ba; Tt = Si-Pb. Deuterides were prepared under the same conditions.

Sample	H$_2$-pressure/ bar	temperature/ K	time/ h	hydride	molar content by EDX	
					Ae	Tt
BaSi	90	450	24	BaSiH$_{2-x}$	51(3)%	48(3)% [a]
SrGe	50	470	10	SrGeH$_{4/3-x}$	47(2)%	53(2)% [a]
SrSn	50	720	10	no reaction		
BaSn	50	470	10	BaSnH$_{4/3-x}$	51.5(7)%	48.5(7)% [b]
SrPb	50	550	2	decomposition to SrPb$_3$ + SrH$_2$		
BaPb	50	570	2	decomposition to Ba$_3$Pb$_5$ + BaH$_2$		

[a]TEM-EDX
[b]SEM-EDX

Characterization

Laboratory powder X-ray diffraction (PXRD) was used to monitor phase purity of the precursor Zintl phases as well as hydride formation. Measurements were done on a Huber G670 diffractometer in Guinier geometry and with copper $K_{\alpha 1}$ radiation. Flat samples were prepared by grinding the moisture sensitive powders in an argon atmosphere, mixing with grease, and putting the sample between two sheets of capton foil.

Powder neutron diffraction (PND) was performed at Institut Laue Langevin (ILL), Grenoble, France at the high-intensity diffractometer D20.[31] Measurements were done at a take off angle of 120° and a wavelength of λ = 1.86613(16) Å or a take off angle of 90° and λ = 2.41538(19) Å. Wavelengths were calibrated using silicon-NIST640b as an external standard. Samples were loaded in an argon filled glovebox with oxygen and moisture content below 1 ppm each. Measurements were done in indium sealed vanadium containers with 6 mm inner diameter at a temperature of 297(2) K.

Powder synchrotron diffraction (PSD) was done using the mail-in service of the Advanced Photon Source (APS), Argonne, USA. Measurements were performed at 11-BM beamline at a wavelength λ = 0.458997 Å and 295 K. Samples were sealed in glass capillaries of 0.3 mm inner diameter which were placed in 0.8 mm capton tubes.

Rietveld refinement [32,33] was done using the TOPAS$^{©}$ software package[34] for synchrotron data. The Stephens model[35] for anisotropic line broadening was used. FULLPROF[36,37] software package was used for neutron diffraction data.

Structure pictures were prepared by VESTA.[38,39] Structural data were normalized using STRUCTURE TIDY[40] as implemented in VESTA.

Solid-State Nuclear Magnetic Resonance (SSNMR) measurements of powdered samples sealed under argon atmosphere in glass tubes were carried out in static magnetic

fields of 9.4 T, 11.7 T, and 17.6 T with *BRUKER AVANCE* spectrometers. Both, a static home-built and BRUKER 4 mm and 2.5 mm MAS probes were used. Static spectra were recorded with a solid-echo sequence[41,42] ($\pi/2$ pulse length 3 μs, recycle delay 500 s). For exciting free induction decays under MAS the pulse length was 5 μs (recycle delay 500 s) and the spinning frequencies were 1.5 kHz and 25 kHz at 11.7 T and 17.6 T, respectively. For data analysis we used either *BRUKER Topspin* or *ORIGINLab* software. Measurements were done on the ^{2}H nucleus of the Zintl phase deuterides $SrGeD_{4/3-x}$ and $BaSiD_{2-x}$. Deuterated water ($D_2O = {}^2H_2O$) was used for setup optimization and referencing. Chemical shifts are given on the δ-scale in regard to TMS.

Energy dispersive X-ray spectroscopy (EDX) was done for chemical analysis of the heavy atoms of the hydrides (deuterides). Either an EDX INCA SYSTEM from Oxford Instruments mounted on a Zeiss LEO 1530 scanning electron microscope (SEM) with 20 kV acceleration voltage and a working distance of 15 mm or an EDAX EDX system mounted on a Philips STEM CM 200 ST transmission electron microscope (TEM) was used.

Quantum Chemical Calculations were done using the QUANTUM ESPRESSO package.[43,44] Calculations were performed in the DFT framework applying the generalized gradient approximation (GGA) and the functional from Perdew-Burke-Ernzerhof (PBE).[45] The projector augmented wave method (PAW)[46] was used and base sets were obtained from the PSlibrary.[47] The plane wave kinetical energy cutoff was tested on convergence and set to 60 ry. Marzari-Vanderbilt cold smearing[48] was used with 0.005 ry for structure relaxations. Density of states (DOS) calculations were done on relaxed structures using the tetrahedron method.[49] Partial density of states (pDOS) were calculated using Gaussian smearing since the tetrahedron method is not implemented.

Hydrogen free Zintl phases were constructed without applying a superstructure. All hydride structures were set in a three-fold superstructure regarding to the parent Zintl phase. An idealized hydrogen content neglecting any nonstoichiometry effect as obtained by neutron

diffraction was used. Structures as well as lattice parameters were relaxed without applying any symmetry restraints but all unit cell angles were constraint to 90°. Density of states (DOS) calculations were done on the relaxed structures. After structure relaxation a pseudo-symmetry search using the PSEUDO module[50–52] of Bilbao Crystallographic Server[53–56] was done. Structural data of the structure relaxations can be found in the supplementary information (Tab. S2, Tab. S4). They are given in the high symmetry setting as obtained from the pseudo-symmetry search. For hydrides the k-space was sampled over a 4 x 4 x 12 mesh for structural relaxations and a 8 x 8 x 24 mesh for an electronic structure calculation on the final structures. Structure relaxation of the hydrogen free Zintl phases were done on a 12 x 4 x 12 mesh. The grids were produced according to the Monkhorst-Pack scheme.[57]

Results

The Zintl phases BaSi, SrGe, as well as AeTt, Ae = Sr, Ba and Tt = Sn, Pb, were attempted to hydrogenate or deuterate (Tab. 1). BaSi forms a hydride (deuteride) phase as described in the literature.[27] In the following a structure model for this phase will be presented. SrGe and BaSn form new hydride (deuteride) phases that are structurally closely related to the CaSiH$_{1.3}$ structure type[24]. SrSn shows no reactivity towards hydrogen, while SrPb and BaPb decompose under formation of SrH$_2$ and SrPb$_3$ or BaH$_2$ and Ba$_3$Pb$_5$, respectively.

Crystal structures of BaSiD$_{2-x}$, SrGeD$_{4/3-x}$ and BaSnD$_{4/3-x}$

The PXRD patterns of the hydrides (deuterides) BaSiD$_{2-x}$, SrGeD$_{4/3-x}$ and BaSnD$_{4/3-x}$ can be indexed in the orthorhombic crystal system. BaSi was hydrogenated by Armbruster *et. al.* before.[26,27] They could index the powder pattern but did not present a structure solution due to poor crystallinity. We reinvestigated BaSiD$_{2-x}$ and extended the scheme to SrGeD$_{4/3-x}$ and BaSnD$_{4/3-x}$. The corresponding Zintl phases, AeTt, Ae = alkaline earth metal, Tt =

tetrel element, crystallize in the orthorhombic CrB-structure type and the Tt-polyanion can be described with the Zintl concept as infinite linear Tt^{2-}-chains.

The hydride (deuteride) phases can be described in a metrically distorted cell of the parent structure. **Thus, in the following, all structures are discussed with regard to the corresponding Zintl phases. For the sake of simplicity all space groups are set with the same axes system as the Zintl phase, e.g., Tt-zig-zag chains run along the crystallographic c axis. Standard settings are given in brackets.** (For the cell transformation see Tab. 4)

Synchrotron and neutron diffraction data suggest space group type $Pbnm$ (No. 62, $Pnma$) for $BaSiD_{2-x}$, $SrGeD_{4/3-x}$ and $BaSnD_{4/3-x}$. For the latter two the crystallographic a axis is tripled with respect to the Zintl phase. The crystal structures of all three compounds could be solved and refined from powder data (Fig. 2). For details of the structure determination and synchrotron powder patterns (Fig. S1 and Fig. S2) please see the supplementary information.

In general the structures of these Zintl phase hydrides show features of interstitial as well as polyanionic hydrides. There is one Ae_4-tetrahedral void per alkaline-earth metal. In addition, voids between the Tt-chains may be occupied as well resulting in a Tt-H bond, which is confirmed by calculations and fits the SSNMR data well. In the following, two distinct structure types resulting from different occupation of such voids will be described in detail.

Table 2: Structural parameters of $BaSiD_{2-x}$, x = 0.13(2) in space group type $Pbnm$ (No 62, $Pnma$) from Rietveld refinement on powder neutron diffraction data. Debye-Waller factors for Ba and Si are fixed to reasonable values.

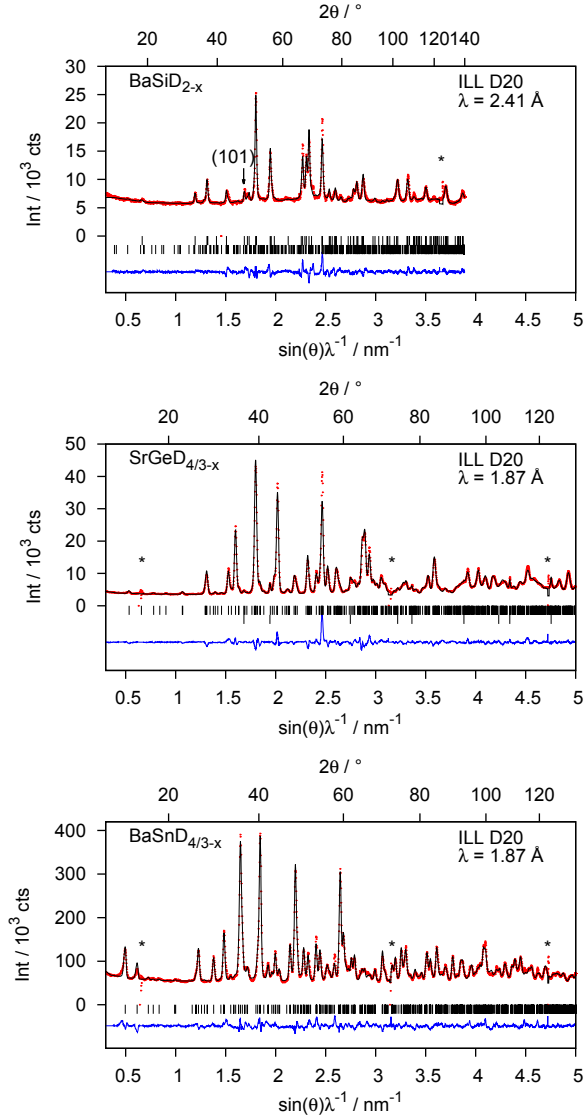|		$BaSiD_{2-x}$, x = 0.13(2)				
		$Pbnm$ (No. 62), $a = 4.4732(8)$ Å, $b = 15.622(2)$ Å, $c = 4.1112(7)$ Å				
Atom	Wyckoff	x	y	z	$B_{iso}/Å^2$	SOF
Ba1	$4c$	0.0060(20)	0.3496(5)	1/4	0.3	1
Si1	$4c$	0.01044(20)	0.0448(8)	1/4	0.7	1
D1	$4c$	0.5100(20)	0.2566(4)	1/4	3.1(3)	0.948(12)
D2	$4c$	0.3773(11)	0.0442(6)	1/4	2.4(3)	0.914(12)

9

Figure 2: Rietveld refinement of the crystal structures of $BaSiD_{2-x}$, x = 0.13(2), $SrGeD_{4/3-x}$, x = 0.139(3) and $BaSnD_{4/3-x}$, x = 0.055(2) using powder neutron diffraction data. (*) excluded due to detector failure. **$BaSiD_{2-x}$:** R_p = 3.02%, R_{wp} = 4.12%, R_{Bragg} = 6.29%, GoF = 2.35; **$SrGeD_{4/3-x}$:** R_p = 4.13%, R_{wp} = 5.59%, R_{Bragg} = 4.46%, GoF = 4.63. **$BaSnD_{4/3-x}$:** R_p = 3.58%, R_{wp} = 4.62%, R_{Bragg} = 5.63%, GoF = 2.06.

10

BaSiD$_{2-x}$: BaSiD$_{2-x}$, x=0.13(2) has the highest hydrogen (deuterium) content within the AeTt-H system and represents a new structure type. The deuterium content is much lower than the literature value of BaSiH$_{3.4}$.[26,27] The structure may be described in space group type *Pbnm* (No. 62, *Pnma*) and does not show any superstructure with regard to the parent Zintl phase. There are two deuterium positions. The deuterium site in the tetrahedral Ba$_4$-void is refined to 95% occupation (Tab. 2, D1). Crystal chemical consideration suggest an additional deuterium atom that binds to the Si-chain and forms a $_1^\infty$[(SiH)$^-$] moiety. This additional site (Tab. 2, D2) was refined to 91% occupation.

The Si-Si chain shows a bond length (DFT calculated values in brackets) of 2.489(10) Å [2.483 Å] and an Si-Si-Si angle of 111.4(4)° [112.0°]. The silicon-hydrogen (deuterium) distance is 1.641(5) Å [1.573 Å]. The H(D)-Si-Si angle is 92.0(3)° [93.1°]. Fig. 3 shows the polyanionic partial structure as well as different projections of the crystal structure.

SrGeD$_{4/3-x}$ and BaSnD$_{4/3-x}$: We describe the compounds SrGeD$_{4/3-x}$ with x = 0.139(3) and BaSnD$_{4/3-x}$ with x = 0.055(2). They show a three-fold superstructure with regard to the Zintl phase and are isotypic to the CaSiH$_{1.3}$ structure type[24]. The structures may be described in space group type *Pbnm* (No. 62, *Pnma*). Structural data are summarized in Tab. 3.

The tetrahedral Ae$_4$-voids are fully occupied with deuterium. The tetrel chains are tilted with respect to the Zintl phase and three of them are connected by an additional Tt-Tt bond (DFT in brackets) with d(Ge2-Ge3) = 2.743(6) Å [2.695 Å] and d(Sn2-Sn3) = 3.085(8) Å [3.052 Å] (Fig. 3). In zig-zag chain direction (*c* direction regarding *Pbnm* setting) the bonds are d(Ge1-Ge2) = 2.551(5) Å [2.556 Å] or d(Sn1-Sn2) = 2.893(7) Å [2.922 Å] (hydrogen terminated chain) and d(Ge3-Ge3) = 2.547(4) Å [2.577 Å] or d(Sn3-Sn3) = 2.965(6) Å [2.941 Å] (middle chain). Thus, the tetrel atoms form condensed six rings in boat configuration (see Fig. 3). There are two condensed boats running in an infinite chain in crystallographic *c* direction, which are hydrogen (deuterium) terminated (D4 site) forming a

Table 3: Structural parameters of SrGeD$_{4/3-x}$, x = 0.139(3), *Pbnm* (No 62, *Pnma*) and BaSnD$_{4/3-x}$, x = 0.055(2), *Pbnm* (No 62, *Pnma*) as obtained by Rietveld refinement using powder neutron diffraction data. Debye-Waller factors were constraint for equal elements. For deuterium occupying tetrahedral voids the site occupancy factor refined to 1.0 within 1 e.s.u., thus, occupation was fixed to 1 during the last refinement cycle.

Atom	Wyckoff	x	y	z	$B_{iso}/Å^2$	SOF
SrGeD$_{4/3-x}$, x = 0.139(3)						
Pbnm (No. 62), a = 11.9113(9) Å, b = 15.2692(11) Å, c = 4.0600(2) Å						
Sr1	4c	0.3414(6)	0.3152(4)	1/4	0.35(9)	1
Sr2	4c	0.6480(6)	0.3397(3)	1/4	0.35	1
Sr3	4c	0.0122(4)	0.3655(4)	1/4	0.35	1
Ge1	4c	0.3125(3)	0.0469(4)	1/4	0.66(7)	1
Ge2	4c	0.7409(3)	0.0403(4)	1/4	0.66	1
Ge3	4c	0.5287(4)	0.5451(3)	1/4	0.66	1
D1	4c	0.5040(5)	0.2240(4)	1/4	1.21(10)	1
D2	4c	0.1570(6)	0.2546(4)	1/4	1.21	1
D3	4c	0.8382(6)	0.2765(4)	1/4	1.21	1
D4	4c	0.4397(7)	0.0380(8)	1/4	1.21	0.592(8)
BaSnD$_{4/3-x}$, x = 0.055(2)						
Pbnm (No. 62), a = 12.9169(7) Å, b = 16.3097(10) Å, c = 4.5554(2) Å						
Ba1	4c	0.3461(7)	0.3075(4)	1/4	0.94(13)	1
Ba2	4c	0.6520(7)	0.3323(4)	1/4	0.94	1
Ba3	4c	0.0156(6)	0.3697(5)	1/4	0.94	1
Sn1	4c	0.3026(4)	0.0527(5)	1/4	1.02(11)	1
Sn2	4c	0.7308(4)	0.0533(5)	1/4	1.02	1
Sn3	4c	0.5303(5)	0.5530(4)	1/4	1.02	1
D1	4c	0.5014(7)	0.2208(3)	1/4	1.92(11)	1
D2	4c	0.1581(6)	0.2531(4)	1/4	1.92	1
D3	4c	0.8410(6)	0.2787(4)	1/4	1.92	1
D4	4c	0.4447(5)	0.0357(5)	1/4	1.92	0.834(6)

$^{\infty}_1$[D-(Ge)$_6$-D] moiety. This D4 site is not fully occupied with SOF = 59% (SrGeD$_{4/3-x}$) and 83% (BaSnD$_{4/3-x}$). The angles in chain connecting direction are 105.54(13)° [100.3 °] (Ge1-Ge2-Ge3) and 104.76(16)° [106.6°] (Ge2-Ge3-Ge3) and 101.8(3)° [96.3°] (D4-Ge1-Ge2) or 98.52(14)° [99.5°] (Sn1-Sn2-Sn3) and 105.41(16)° [105.6°] (Sn2-Sn3-Sn3) and 93.3(2)° [94.0 °] (D4-Sn1-Sn2). In chain direction the angles are 107.9(3)° [103.8 °] (Ge1-Ge2-Ge1) and 105.68(18) ° [102.5°] (Ge3-Ge3-Ge3) and for the corresponding BaSnD$_{4/3-x}$ compound angles are 103.9(3)° [102.4 °] (Sn1-Sn2-Sn1) and 100.37(18) ° [101.6°] (Sn3-Sn3-Sn3). Fig. 3 shows the polyanionic partial structure as well as different projections of the crystal structure including the labeling of the polyanion.
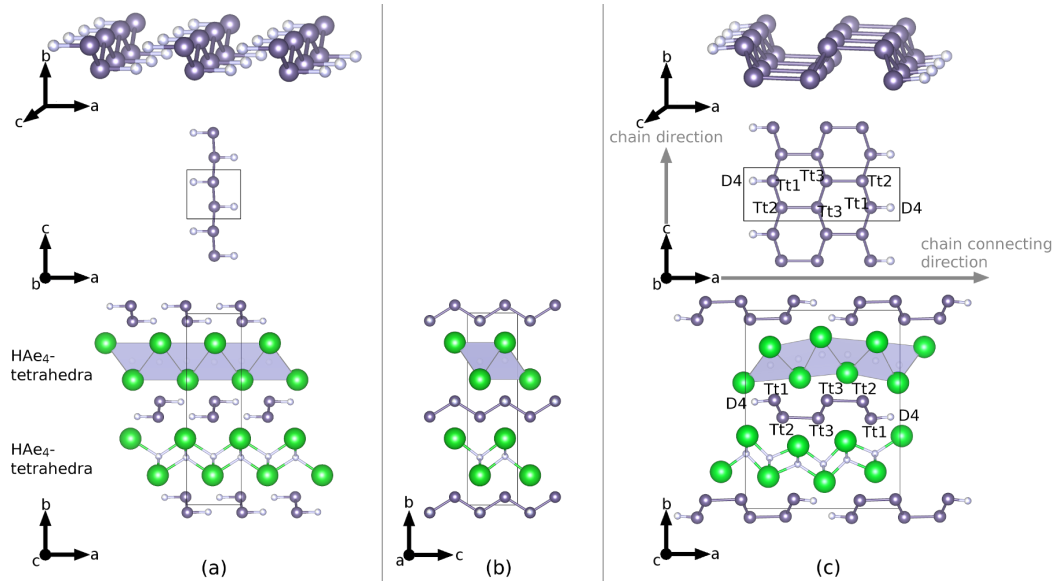

Figure 3: Different projections of the polyanion as well as the crystal structure of **(a,b)** BaSiD$_{2-x}$ and **(c)** AeTtD$_{4/3-x}$ (SrGeD$_{4/3-x}$ and BaSnD$_{4/3-x}$). **(b)** shows the [100] view of BaSiD$_{2-x}$ to emphasize on the tetrahedral voids and the zig-zag chains. This projection looks similar for both structure types. **Large spheres**: Alkaline earth metal (Ae); **medium spheres**: Tetrel element (Tt); **small spheres**: Hydrogen/deuterium (H/D).

Density of States (DOS)

All presented compounds are non-stoichiometric Zintl phase hydrides. For DFT calculations an idealized composition of AeTtH$_n$, n = 4/3 (SrGeH$_n$, BaSnH$_n$), 2 (BaSiH$_n$) was used. Then they can formally be considered to be comprised of ions Ae^{2+} + H$^-$ + (n-1)(TtH)$^-$ +

Table 4: Lattice parameters of the Zintl phases BaSi, SrGe, BaSn and their corresponding deuterides. The unit cell volume is normalized to formula units (fu).

Compound	x =	Spgr.	Super-str.[a] a =	Lattice parameter			V/fu / Å³
				a / Å	b / Å	c / Å	
silicides							
BaSi[58]		*Cmcm*		5.0430(8)	11.933(2)	4.1395(8)	62.3
BaSi		*Cmcm*		5.0342(2)	11.9171(3)	4.1335(2)	62.0
BaSi [b]		*Cmcm*		4.953	11.961	4.085	60.5
BaSiH$_{3.4}$		*Pbnm* [c]	$3\tilde{a}$	13.43(8)	15.73(15)	4.13(3)	72.7
BaSiD$_{2-x}$ [d]		*Cmcm*	none	4.48485(5)	15.66599(18)	4.12256(3)	72.4
BaSiD$_{2-x}$ [e]	0.13(2)	*Pbnm* [c]	none	4.4732(8)	15.622(2)	4.1112(7)	71.8
BaSiD$_2$ [b]			none [f]	4.3996	15.332	4.1156	69.3
germanides							
SrGe[59]		*Cmcm*		4.820(5)	11.39(1)	4.167(2)	57.0
SrGe		*Cmcm*		4.82389(6)	11.37955(11)	4.17265(4)	57.3
SrGe [b]		*Cmcm*		4.756	11.325	4.143	55.8
SrGeD$_{4/3-x}$ [d]		*Pbnm* [c]	$3\tilde{a}$	11.84848(12)	15.3938(2)	4.06561(4)	61.8
SrGeD$_{4/3-x}$ [e]	0.139(3)	*Pbnm* [c]	$3\tilde{a}$	11.9113(9)	15.2692(11)	4.0600(2)	61.5
SrGeD$_{4/3}$ [b]			$3\tilde{a}$	11.624	15.152	4.046	59.4
stannides							
BaSn[59]		*Cmcm*		5.316(5)	12.55(1)	4.657(2)	77.7
BaSn		*Cmcm*		5.3168(2)	12.5037(5)	4.6534(2)	77.3
BaSn [b]		*Cmcm*		5.263	12.537	4.644	76.6
BaSnD$_{4/3-x}$ [e]	0.055(2)	*Pbnm* [c]	$3\tilde{a}$	12.9169(7)	16.3097(10)	4.5554(2)	80.0
BaSnD$_{4/3}$ [b]			$3\tilde{a}$	12.814	16.034	4.5564	78.0

[a] $\tilde{a}$ refers to the basis structure of the parent Zintl phase.
[b] DFT; for calculated structures an ideal occupation was assumed.
[c] nonstandard setting, standard setting is *Pnma* with $a' = b$, $b' = c$ and $c' = a$.
[d] synchrotron diffraction
[e] neutron diffraction
[f] structure relaxation using $a = 3\tilde{a}$; From a pseudo symmetry search a smaller cell was obtained.

(2-n)Tt$^-$. DOS calculations were preformed on these idealized structures without vacancies in the hydrogen partial structure. The Zintl like view is supported by the DOS. SrGeH$_{4/3}$ and BaSnH$_{4/3}$ show a small band gap while BaSiH$_2$ is a poor metal with a pseudo-gap at the Fermi level (Fig. 4). Partial-DOS for SrGeH$_{4/3}$ and BaSiH$_2$ are shown in Fig. 5 for selected atoms and orbitals. The s-band of hydrogen atoms in tetrahedral Ae$_4$-voids shows only a low dispersion and lies below the Fermi level indicating a hydridic species. In contrast, the hydrogen which terminates atoms of the Si(Ge)-chain mix with Si(Ge)-bands and also shows a fraction above the Fermi level. The structure of SrGeH$_{4/3}$ shows Ge-atoms that bind only to three other Ge-atoms and Ge-atoms that bind to both, hydrogen and germanium. The main direction for the interaction with hydrogen is the crystallographic a axis. Thus, the p$_x$ derived bands of the hydrogen terminated Ge-atoms are lowered while the p$_y$ and p$_z$ components as well as all components of the other germanium atoms form bands at higher energies above and below the Fermi level. Since all Si-atoms of BaSiH$_2$ are terminated by hydrogen in a direction all Si-p$_x$ derived bands are lowered. Only the Si-p$_y$ and -p$_z$ derived bands show electron density at the Fermi level.

Solid-state nuclear magnetic resonance (SSNMR)

In Fig. 6 we show the static (a) ^{2}H NMR spectra of BaSiD$_{2-x}$ (*left*) and SrGeD$_{4/3-x}$ (*right*), together with their simulations (b), and low-spinning MAS (c) spectra. For both materials, we observe a narrow line in addition to a broad spectrum. Note that for ^{2}H (spin-1 nucleus) there is no central transition. Thus, the narrow lines for BaSiD$_{2-x}$ (SrGeD$_{4/3-x}$) of 1.3 kHz (3.9 kHz) widths point to nuclear sites with nearly cubic local charge symmetry, i.e., vanishing electric field gradient (EFG). On the other hand, broad powder patterns must originate from ^{2}H nuclei with very different local charge symmetry, which causes a substantial EFG. All widths are found to be independent of the magnetic field in frequency units (data not shown), which points to quadrupolar linewidths for the broad powder pattern, which is also borne out in the slow-spinning MAS spectra (6(c)). The quadrupole frequencies that characterize the
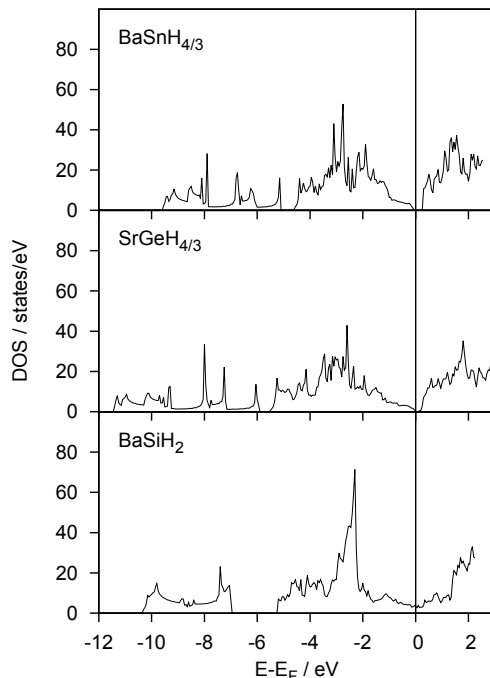
Figure 4: Total density of states (DOS) of hydrides of BaSn, SrGe and BaSi

found isotropic EFGs are 51(1) kHz and 39(1) kHz for $BaSiD_{2-x}$ and $SrGeD_{4/3-x}$, respectively.

Careful evaluations of the relative intensities within each sample revealed ratios of 1:1 ($BaSiD_{2-x}$) and about 3:1 ($SrGeD_{4/3-x}$), for narrow vs. broad spectra. This means, as one can already guess from Fig. 6, that there are three times as many ^2H nuclei occupying the sites of higher charge symmetry in $SrGeD_{4/3-x}$ compared to the crystallographic site that shows a substantial EFG, while for $BaSiD_{2-x}$ the number of nuclei in both type of sites is similar.

The field independent width of the narrow line in $BaSiD_{2-x}$ (1.3 kHz) is in agreement with what one expects from homonuclear dipole-dipole coupling between ^2H nuclei (derived from the crystal structure). The much broader line in $SrGeD_{4/3-x}$ (3.9 kHz), however, is probably caused by a very weak quadrupole coupling (or indirect nuclear coupling), and the subject to further investigation.

Substantial line narrowing under fast MAS (17.6 T, 25 kHz spin rate, not shown) gives isotropic shifts for the nuclei with strong quadrupole coupling of about $\delta = 0$ ppm, while the narrow lines are clearly displaced at $\delta = 11(1)$ ppm with regard to TMS.
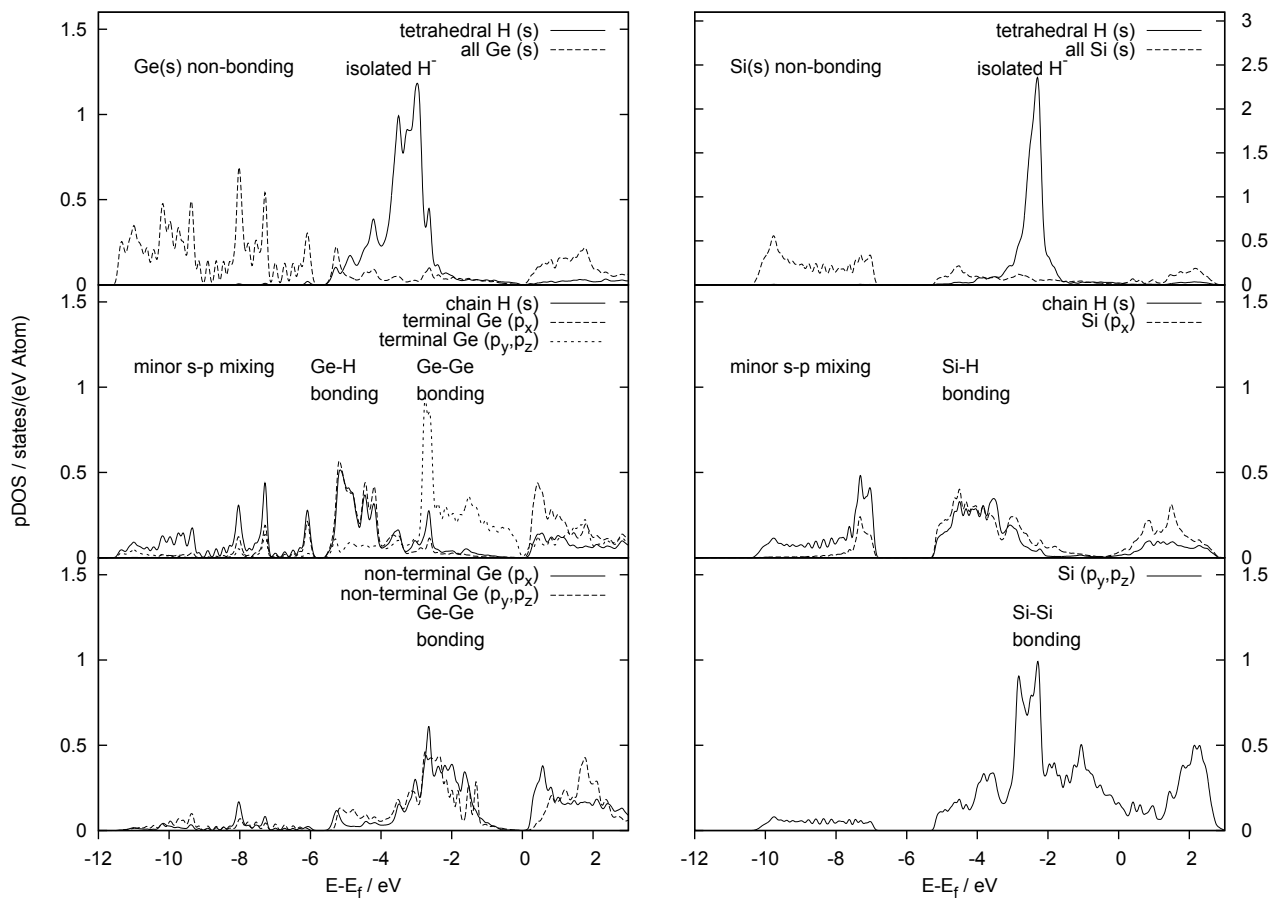
16

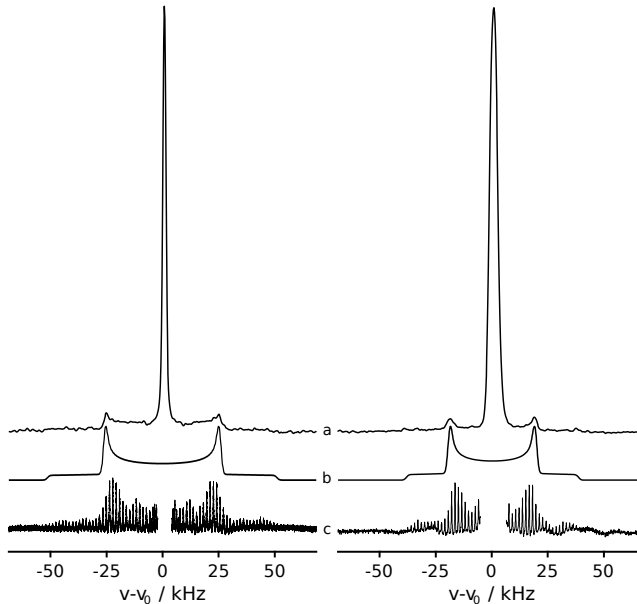Figure 5: Partial density of states (pDOS) for selected atoms and orbitals **Left**: $SrGeH_{4/3}$ **Right**: $BaSiH_2$.

Figure 6: **(a)** Static solid-echo ^{2}H NMR spectra of BaSiD$_{2-x}$ (*left*) and SrGeD$_{4/3-x}$ (*right*) obtained at 9.4 T. **(b)** Simulated first order quadrupole powder pattern that fits the broad component of the static spectra in (a). **(c)** Slow MAS spectra (1.5 kHz) at 11.4 T are in agreement with the assumed powder pattern from quadrupole interaction. The intense central line is cut out for better visualization.

Spin lattice relaxation times on the order of 10^2 s with slight differences among the various resonance lines (at most a factor of two) may be typical for insulating compounds, but a definite assignment of the involved mechanisms is still under investigation.

Discussion

This paper describes two new compounds SrGeD$_{4/3-x}$, x = 0.139(3) and BaSnD$_{4/3-x}$, x = 0.055(2) in the CaSiH$_{1.3}$-structure type and it assigns a new structure type to BaSiD$_{2-x}$, x = 0.13(2). According to the classification of Häussermann[8] these phases show features of interstitial hydrides due to filled tetrahedral Ae$_4$-voids (Ae = Sr, Ba) as well as features of polyanionic hydrides due to short Tt-D (Tt = Si-Sn) distances which according to bond lengths are all in the region of covalent interaction.

The polyanionic partial structure is strongly geometrically constraint since it lies between ionically dominated sheets of edge connected HAe$_4$-tetrahedra. Therefore *a*- and *c*-directions

18

are rigidly coupled to the size of the tetrahedra. A hypothetical AeTtH, Ae = alkaline earth metal, Tt = group 14 element, can be formulated according to the Zintl concept as $Ae^{2+}H^-Tt^-$. Thus, for the group 14 element (Tt^-) we can expect sheets in between the salt like tetrahedral layers similar to the structure of black phosphorus or grey arsenic. Each Tt atom is then covalently bound to three other Tt atoms and the bonds can be suspected to have single bond character. Indeed we find a structure motif of condensed boat configurations in contrast to the armchair configuration in black phosphorus. Due to the rigidity of the salt like layers a totally condensed AeTtH-structure was not obtained yet. To comply with the predetermined required space additional $Tt-H(D)$ bonds are formed (Fig. 3).

In $SrGeD_{4/3-x}$ and $BaSnD_{4/3-x}$ two thirds of the tetrel atoms form an additional Tt-Tt bond compared to the hydrogen (deuterium) free Zintl phase. With this additional bond tetrel atoms form condensed six-rings in boat configuration. In crystallographic a-direction two boats are condensed, while an infinite chain of these double row of boats runs along crystallographic c axis. The last third of the tetrel atoms is hydrogen (deuterium) terminated and therefore separates the condensed boats spatially (Fig. 3). Both compounds are non-stoichiometric and furthermore for $SrGeD_{4/3-x}$ it was shown that x changes slightly over time.[30] The tetrahedral Sr_4- or Ba_4-voids are fully occupied (Tab. 3, D1-D3), but the boat terminating site (Tab. 3, D4) is not fully occupied and thus some germanium/tin atoms are undersaturated. Assuming ideal composition (x = 0) the Zintl concept can be applied giving $Ae^{2+}H^-(Tt^-)_{2/3}((TtH)^-)_{1/3}$.

$BaSiD_{2-x}$ shows a new structure type where the polyanion forms zig-zag $^{\infty}_1[(SiH)^-]$ chains. They are isoelectronic to a poly-phosphane $(PH)_x$, which is claimed to be a non-volatile yellow solid,[60] but proof of its existence is still elusive.[61,62] $BaSiD_{2-x}$ is a non-stoichiometric compound as well with 95% of the tetrahedral Ba_4 voids occupied as well as 91% of the silicon atoms terminated by hydrogen (deuterium). In the ideal composition it could be considered as $Ba^{2+}H^-(SiH)^-$.

All phases show an undersaturation at the Tt-polyanionic backbone, which needs expla-

nation. This non-stoichiometry effect can be rationalized in two ways. First there could be additional Tt-Tt bonds and therefore more extended polyanions, which derive from the current model by further condensation along the crystallographic a direction. In case such larger units would be statistically distributed within the crystal structure, this might result in reduced deuterium occupation as observed in the structure refinements. As an alternative explanation π-bonding in the polyanion may play a role. From DFT calculations of AeSi (Ae = Ca-Ba)[63,64] as well as an experimental charge density study on CaSi[65] it is well known that poor metallic behavior is caused by π-bonding due to Si(p)-Ae(d)-overlap and therefore depopulated π^*-bands. An oxidation by depopulating π^*-bands would result in shortened Tt-Tt bonds within the chains. Experimental data unfortunately do not allow a clear distinction between those two models. In any case Tt-D distances might be affected hereby.

From a structure refinement of neutron diffraction data the Ge-D distance is 1.521(9) Å, which is in the same region as for molecular GeD_4 at low temperatures, while the Sn-D distance of 1.858(8) Å is 8% larger than in molecular SnD_4 at low temperature.[66] Quantum chemical structure relaxation on the idealized compositions shows good agreement for Sn-D with 1.867 Å, but assumes a larger distance for Ge-D with 1.667 Å. The non-stoichiometry should have a larger effect on the calculation of $SrGeD_{4/3-x}$ since x is larger in this case. The Si-D bond length in $BaSiD_{2-x}$, which was determined as 1.641(5) Å, is elongated compared to similar covalently bound Si-D groups like 1.54 Å for β-$KSiD_3$ at low temperature,[17] but a comparable bond length was determined for a hypervalent SiH_6^{2-} moiety.[67] Quantum chemical calculations suggest a 4% shorter Si-D distance, but were done on an idealized composition.

Partial density of states (pDOS) which was calculated for both structure types (i.e. for $BaSiH_2$ and $SrGeH_{4/3}$, Fig. 5) shows a strong difference between the hydrogen located in a tetrahedral alkaline earth void and the hydrogen binding to the tetrel chain. The tetrahedral site shows a sharp band with negligible contribution of electronic states of other atoms. The

pDOS of hydrogen bound to tetrel is highly dispersive and mixes with tetrel states mainly arising from the p_x-orbitals pointing to the hydrogen atom. Thus a bonding interaction is assumed here.

The Ge-Ge distances change over time due to a small deuterium release which is explained in detail in a forthcoming paper.[30] While synchrotron powder diffraction was done on a freshly prepared sample neutron diffraction was done after 70 days. The Ge-Ge bonds of the zig-zag chains as predetermined by the hydrogen (deuterium) free Zintl phase are shortened. Synchrotron diffraction results fit DFT calculated distances (given in square brackets) well with d(Ge1-Ge2) = 2.5720(16) Å [2.556 Å] for the hydrogen (deuterium) terminated chain and d(Ge3-Ge3) = 2.5681(13) Å [2.577 Å] for the middle chain. Neutron diffraction shows a further contraction for the terminal chain with 2.511(5) Å. Therefore the bonds in chain direction are much shorter than in the hydrogen (deuterium) free Zintl phase with 2.6462(16) Å [2.613 Å]. As discussed above this shortening might be caused by depopulating π^*-bands, i. e. oxidation of the Zintl polyanion. Comparing the DFT derived values for the Zintl phase and its hydride confirms this trend (see Tab. S5). The chain connecting bond running in a-direction is strongly elongated (d(Ge2-Ge3) = 2.743(6) Å) compared to the other bonds. The same trend is obtained for $BaSnD_{4/3-x}$ (Tab. S5). The Si-Si chain does not show a significant difference to the hydrogen (deuterium) free Zintl phase. DFT calculated distances on a fully hydrogen terminated Si-chain confirms this. For details see Tab. S5.

The Si-Si-Si angle is 111.4°, while Ge-Ge-Ge and Sn-Sn-Sn angles are systematically smaller in the region of 103.37(8)°-107.9(3)° and 98.52(14)°-105.41(16)°, respectively (Tab. S5). They fit DFT derived angles well and are larger than the angles in black phosphorus (102.09(8)° and 96.64(4)°[68]) or grey arsenic (96.64(6)°[69]) which resemble condensed armchair six-rings. The D-Ge-Ge angle is 101.8(3)° and therefore widened compared to the DFT derived value (96.3°), which might be caused by the non-stoichiometry effect again. The D-Sn-Sn and D-Si-Si angles fit to the DFT value (Tab. S6). These angles are smaller than the corresponding Tt-Tt-Tt angles.

Solid state NMR was performed on the ^{2}H nucleus of $BaSiD_{2-x}$ and $SrGeD_{4/3-x}$ in order to avoid contamination from spurious ^{1}H signals. Based on the structure of the materials it appears unambiguous to assign the different crystallographic sites to our two NMR signals in Fig. 6. The narrow lines represent ^{2}H in the tetrahedral voids that have nearly cubic charge symmetry. Whereas, the broad signals are caused by ^{2}H nuclei attached to Si/Ge atoms. The latter sites are expected to show a substantial axially symmetric quadrupole splitting if chemically bound to Si/Ge (σ-bond). Further experimental proof for this scenario comes from the NMR intensities. For $SrGeD_{4/3-x}$, due to the tilting and the interconnected Ge chains (Fig. 3), the number of ^{2}H atoms enclosed by the Sr_4 tetrahedral voids exceeds that of the Ge chain sites by a factor of about 3. On the other hand, for $BaSiD_{2-x}$ we expect nearly equal numbers of nuclei in either position. More independent confirmation of the assignment comes from the fact that both sites are expected to be rather similar in both materials, and that is what we find from NMR shifts and quadrupole splittings. Thus, there can be no doubt with regard to the site assignment.

Obviously, the vanishing quadrupole splitting is expected for the ^{2}H sites within tetrahedra for symmetry reasons. The different quadrupole splittings (51(1) and 39(1) kHz) for the polyanionic sites fit an expected general trend that σ-bonds involving silicon are stronger than in the case of germanium.

While the width of the narrow line for $BaSiD_{2-x}$ is in good agreement with nuclear dipole-dipole coupling, for $SrGeD_{4/3-x}$ significant additional broadening is present. Since it is field independent, a likely candidate is a weak quadrupole coupling. Indeed, the tetrahedral voids spanned by Sr atoms are much less regular compared to those made up by Ba in $BaSiD_{2-x}$. The resulting distortion is prone to result in a non-vanishing EFG that could explain the observed width.

The chemical shifts are very similar for both materials with a about $\delta = 0$ ppm for the polyanionic site and about $\delta = +11$ ppm for the tetrahedral site referenced to TMS. The perhaps surprisingly large positive shift for hydrogen in the tetrahedral voids is not unusual

since the ^{2}H chemical shift in BaD_2 was reported to be about $\delta = +9$ ppm.[70,71]

Since the nuclear relaxation is rather long and similar in both systems substantial contributions from itinerant carriers are not likely. Furthermore, paramagnetic impurities such as Eu, which are common in strontium and barium, might easily explain the observed relaxation.

Conclusion

In this contribution we show the existence of two new phases $SrGeD_{4/3-x}$ and $BaSnD_{4/3-x}$. Since there are two additional hydrogen (deuterium) poor phases in the $SrGe-H_2$ system (as shown in a forthcoming paper[30]) $SrGeD_{4/3-x}$ will be called γ-$SrGeD_y$ as well. We also reinvestigated the compound $BaSiD_{2-x}$.

The existence of polyanionic hydrides (deuterides) of group 14 elements was questioned. While Ohba *et al.*[24] assume a short Si-H distance of 1.58 Å and thus a covalent bond in $CaSiH_{1.3}$ from synchrotron diffraction as well as DFT calculations, Wu *et al.*[25] found a much longer distance d(Si-D) = 1.82 Å from powder neutron diffraction. They support their view by neutron vibrational spectroscopy.

We now could show the existence of new polymeric main-group element-hydrogen structures with the group 14 elements Si, Ge and Sn. We prepared the deuteride phases $SrGeD_{4/3-x}$ and $BaSnD_{4/3-x}$ that resemble the structure which was proposed by Ohba *et al.*[24] for $CaSiH_{1.3}$. The polyanionic structures show similarities to the elemental structures of black phosphorus or grey arsenic, but, while these elements consist of condensed armchair six-rings, the new structures show a condensed boat motif. It is topologically related to the boron partial structure of OsB_2[72] which is cut by the terminating hydrogen (deuterium) atoms. In addition some of the germanium and tin atoms are terminated by deuterium. The bonding length of d(Ge-D) = 1.521(9) Å [1.667 Å] and d(Sn-D) = 1.858(8) Å [1.867 Å] (DFT calculations in brackets) are clearly in a region of covalent bonding.

In the structure of $BaSiD_{2-x}$ the zig-zag Si^{2-} chain as in the parent Zintl phase BaSi is retained. However it is terminated by hydrogen (deuterium) (except for the non-stoichiometry) forming a linear $(SiH)^{-}$-chain as we would expect from a poly-phosphane. The distance d(Si-D) = 1.641(5) Å as obtained from neutron diffraction (DFT: d = 1.573 Å) is larger than the value proposed for $CaSiH_{1.3}$ by Ohba *et al.*[24] but much shorter than the value Wu *et al.*[25] determined by neutron diffraction for $CaSiD_{1.2}$.

We also applied solid-state NMR to $BaSiD_{2-x}$ and $SrGeD_{4/3-x}$ and could distinguish and assign two chemically different sites. The quadrupolar interaction of the ^2H nuclei bound to Si/Ge atoms fits into the picture of a covalent bond. Therefore we can show the first well confirmed polyanionic hydrides of group 14 elements.

Dedication

Dedicated to Prof. Lothar Beyer on the occasion of his 80th birthday.

Supporting Information Available

The following files are available free of charge.

Technical information on the evaluation of diffraction data. Rietveld plots derived from synchrotron diffraction (Fig. S1, S2). Structural parameters as refined from synchrotron diffraction as well as calculated by DFT structure relaxations (Tab. S1-S4). A list of Tt-Tt distances and Tt-Tt-Tt angles (Tab. S5). A list of Tt-D distances and Tt-Tt-D angles (Tab. S6). CIF files ($BaSiD_{1.86}$, $SrGeD_{1.20}$, $BaSnD_{1.28}$ in standard setting, please consider the rotation of the axes system) from neutron diffraction data.

Acknowledgement

References

(1) Zintl, E.; Kaiser, H. Über die Fähigkeit der Elemente zur Bildung negativer Ionen. *Z. Anorg. Allg. Chem.* **1933**, *211*, 113–131.

(2) Zintl, E. Intermetallische Verbindungen. *Angew. Chem.* **1939**, *52*, 1–6.

(3) Schäfer, H.; Eisenmann, B.; Müller, W. Zintl-Phasen: Übergangsformen zwischen Metall- und Ionenbindung. *Angew. Chem.* **1973**, *85*, 742–760.

(4) Schäfer, H. On the Problem of Polar Intermetallic Compounds: The Stimulation of E. Zintl's Work for the Modern Chemistry of Intermetallics. *Annu. Rev. Mater. Sci.* **1985**, *15*, 1–42.

(5) Nesper, R. Chemische Bindungen - Intermetallische Verbindungen. *Angew. Chem.* **1991**, *103*, 805–834.

(6) Corbett, J. D. Polyanionic Clusters and Networks of the Early p-Element Metals in the Solid State: Beyond the Zintl Boundary. *Angew. Chem., Int. Ed.* **2000**, *39*, 670–690.

(7) Nesper, R. The Zintl-Klemm Concept A Historical Survey. *Z. Anorg. Allg. Chem.* **2014**, *640*, 2639–2648.

(8) Häussermann, U.; Kranak, V. F.; Puhakainen, K. In *Zintl Phases*; Fässler, T. F., Ed.; Structure and Bonding; Springer Berlin Heidelberg, 2011; Vol. 139; pp 143–161.

(9) Fahlquist, H.; Noréus, D.; Callear, S.; David, W. I. F.; Hauback, B. C. Two New Cluster Ions, $Ga[GaH_3]_4^{5-}$ with a Neopentane Structure in $Rb_8Ga_5H_{15}$ and $[GaH_2]_n^{n-}$ with a Polyethylene Structure in $Rb_n(GaH_2)_n$, Represent a New Class of Compounds with Direct Ga-Ga Bonds Mimicking Common Hydrocarbons. *J. Am. Chem. Soc.* **2011**, *133*, 14574–14577.

(10) Fahlquist, H.; Noréus, D. $Cs_{10}H[Ga_3H_8]_3$: A Hydrogenous Zintl phase Containing Propane-Like Polyanions $[Ga_3H_8]^{3-}$ and Interstitial Hydrogen. *Inorg. Chem.* **2013**, *52*, 7125–7129.

(11) Fahlquist, H.; Noréus, D.; Sørby, M. H. Varying the Alkali-Metal Radii in $(K_xRb_{1x})_n[GaH_2]_n$ ($0 \leq x \leq 1$) Reorients a Stable Polyethylene-Structured $[GaH_2]_n^n$ Anionic Chain. *Inorg. Chem.* **2013**, *52*, 4771–4773.

(12) Gingl, F.; Vogt, T.; Akiba, E. Trigonal $SrAl_2H_2$: the first Zintl phase hydride. *J. Alloys Comp.* **2000**, *306*, 127 – 132.

(13) Björling, T.; Noréus, D.; Häussermann, U. Polyanionic Hydrides from Polar Intermetallics AeE_2 (Ae = Ca, Sr, Ba; E = Al, Ga, In). *J. Am. Chem. Soc.* **2006**, *128*, 817–824.

(14) Wenderoth, P.; Kohlmann, H. In Situ Neutron Powder Diffraction of the Formation of $SrGa_2D_2$, and Hydrogenation Behavior of $YbGa_2$ and $EuGa_2$. *Inorg. Chem.* **2013**, *52*, 10525–10531.

(15) Chotard, J.-N.; Tang, W. S.; Raybaud, P.; Janot, R. Potassium Silanide ($KSiH_3$): A Reversible Hydrogen Storage Material. *Chem. - Eur. J.* **2011**, *17*, 12302–12309.

(16) Tang, W. S.; Chotard, J.-N.; Raybaud, P.; Janot, R. Hydrogenation properties of KSi and NaSi Zintl phases. *Phys. Chem. Chem. Phys.* **2012**, *14*, 13319–13324.

(17) Tang, W. S.; Chotard, J.-N.; Raybaud, P.; Janot, R. Enthalpy-Entropy Compensation Effect in Hydrogen Storage Materials: The Striking Example of Alkali Silanides $MSiH_3$ (M=K, Rb, Cs). *J. Phys. Chem. C* **2014**, *118*, 3409–3419.

(18) Kranak, V. F.; Lin, Y.-C.; Karlsson, M.; Mink, J.; Norberg, S. T.; Häussermann, U. Structural and Vibrational Properties of Silyl (SiH_3^-) Anions in $KSiH_3$ and $RbSiH_3$: New Insight into SiH Interactions. *Inorg. Chem.* **2015**, *54*, 2300–2309.

(19) Kranak, V. F.; Benson, D. E.; Wollmann, L.; Mesgar, M.; Shafeie, S.; Grins, J.; Häussermann, U. Hydrogenous Zintl Phase $Ba_3Si_4H_x$ (x = 1-2): Transforming Si_4 Butterfly Anions into Tetrahedral Moieties. *Inorg. Chem.* **2015**, *54*, 756–764.

(20) Evans, M. J.; Holland, G. P.; Garcia-Garcia, F. J.; Häussermann, U. Polyanionic Gallium Hydrides from AlB_2-Type Precursors AeGaE (Ae = Ca, Sr, Ba; E = Si, Ge, Sn). *J. Am. Chem. Soc.* **2008**, *130*, 12139–12147.

(21) Evans, M. J.; Kranak, V. F.; Garcia-Garcia, F. J.; Holland, G. P.; Daemen, L. L.; Proffen, T.; Lee, M. H.; Sankey, O. F.; Häussermann, U. Structural and Dynamic Properties of BaInGeH: A Rare Solid-State Indium Hydride. *Inorg. Chem.* **2009**, *48*, 5602–5604.

(22) Lee, M. H.; Björling, T.; Hauback, B. C.; Utsumi, T.; Moser, D.; Bull, D.; Noréus, D.; Sankey, O. F.; Häussermann, U. Crystal structure, electronic structure, and vibrational properties of MAlSiH ($M = $ Ca, Sr, Ba): Hydrogenation-induced semiconductors from the AlB_2-type alloys MAlSi. *Phys. Rev. B* **2008**, *78*, 195209.

(23) Kranak, V. F.; Evans, M. J.; Daemen, L. L.; Proffen, T.; Lee, M. H.; Sankey, O. F.; Häussermann, U. Structural and dynamic properties of the polyanionic hydrides SrAl-GeH and BaAlGeH. *Solid State Sci.* **2009**, *11*, 1847 – 1853.

(24) Ohba, N.; Aoki, M.; Noritake, T.; Miwa, K.; Towata, S.-i. First-principles study of a hydrogen storage material CaSi. *Phys. Rev. B* **2005**, *72*, 075104.

(25) Wu, H.; Zhou, W.; Udovic, T. J.; Rush, J. J.; Yildirim, T. Structure and hydrogen bonding in $CaSiD_{1+x}$ Issues about covalent bonding. *Phys. Rev. B* **2006**, *74*, 224101.

(26) Armbruster, M. M. Reaktionen von Wasserstoff mit Zintl-Phasen. Dissertation, Eidgenössische Technische Hochschule (ETH) Zürich, 2008.

(27) Armbruster, M.; Wörle, M.; Krumeich, F.; Nesper, R. Structure and Properties of Hydrogenated Ca, Sr, Ba, and Eu Silicides. *Z. Anorg. Allg. Chem.* **2009**, *635*, 1758–1766.

(28) Ångström, J.; Johansson, R.; Sarkar, T.; Sørby, M. H.; Zlotea, C.; Andersson, M. S.; Nordblad, P.; Scheicher, R. H.; Häussermann, U.; Sahlberg, M. Hydrogenation-Induced Structure and Property Changes in the Rare-Earth Metal Gallide NdGa: Evolution of a $[GaH]^2$ Polyanion Containing Peierls-like GaH Chains. *Inorg. Chem.* **2016**, *55*, 345–352.

(29) Nedumkandathil, R.; Kranak, V. F.; Johansson, R.; Ångström, J.; Balmes, O.; Andersson, M. S.; Nordblad, P.; Scheicher, R. H.; Sahlberg, M.; Häussermann, U. Hydrogenation Induced Structure and Property Changes in GdGa. *J. Solid State Chem.* **2016**, *239*, 184 – 191.

(30) Auer, H.; Wallacher, D.; Hansen, T.; Kohlmann, H. Hydrides of Alkaline-earth-Tetrel (AeTt) Zintl Phases: *in situ* Hydrogenation - Phases in the $SrGe-D_2$ System. *submitted to Inorg. Chem.* **2016**,

(31) Hansen, T. C.; Henry, P. F.; Fischer, H. E.; Torregrossa, J.; Convert, P. The D20 instrument at the ILL: a versatile high-intensity two-axis neutron diffractometer. *Meas. Sci. and Technol.* **2008**, *19*, 034001.

(32) Rietveld, H. M. Line profiles of neutron powder-diffraction peaks for structure refinement. *Acta Crystallogr.* **1967**, *22*, 151–152.

(33) Rietveld, H. M. A profile refinement method for nuclear and magnetic structures. *J. Appl. Crystallogr.* **1969**, *2*, 65–71.

(34) Bruker AXS, TOPAS© version 5, www.bruker-axs.com.

(35) Stephens, P. W. Phenomenological model of anisotropic peak broadening in powder diffraction. *J. Appl. Crystallogr.* **1999**, *32*, 281–289.

(36) Rodríguez-Carvajal, J. Recent advances in magnetic structure determination by neutron powder diffraction. *Phys. B* **1993**, *192*, 55 – 69.

(37) Rodríguez-Carvajal, J. FullProf.2k, Version 5.30 - Mar2012-ILL JRC. 2012.

(38) Momma, K.; Izumi, F. *VESTA3* for three-dimensional visualization of crystal, volumetric and morphology data. *J. Appl. Crystallogr.* **2011**, *44*, 1272–1276.

(39) VESTA - Visualisation for Electronic and STructural Analysis, version 3.3.1.

(40) Gelato, L. M.; Parthé, E. *STRUCTURE TIDY* – a computer program to standardize crystal structure data. *J. Appl. Crystallogr.* **1987**, *20*, 139–143.

(41) Hahn, E. L. Spin echoes. *Phys. Rev.* **1950**, *80*, 580.

(42) Powles, J.; Mansfield, P. Double-pulse nuclear-resonance transients in solids. *Phys. Lett.* **1962**, *2*, 58–59.

(43) Giannozzi, P. et al. QUANTUM ESPRESSO: a modular and open-source software project for quantum simulations of materials. *J. Phys.: Condens. Matter* **2009**, *21*, 395502 (19pp).

(44) http://www.quantum-espresso.org, QUANTUM ESPRESSO v. 5.1.2.

(45) Perdew, J. P.; Burke, K.; Ernzerhof, M. Generalized Gradient Approximation Made Simple. *Phys. Rev. Lett.* **1996**, *77*, 3865–3868.

(46) Blöchl, P. E. Projector augmented-wave method. *Phys. Rev. B* **1994**, *50*, 17953–17979.

(47) http://www.qe-forge.org/gf/project/pslibrary, version 0.3.1.

(48) Marzari, N.; Vanderbilt, D.; De Vita, A.; Payne, M. C. Thermal Contraction and Disordering of the Al(110) Surface. *Phys. Rev. Lett.* **1999**, *82*, 3296–3299.

(49) Blöchl, P. E.; Jepsen, O.; Andersen, O. K. Improved tetrahedron method for Brillouin-zone integrations. *Phys. Rev. B* **1994**, *49*, 16223–16233.

(50) Kroumova, E.; Aroyo, M. I.; Perez-Mato, J. M.; Ivantchev, S.; Igartua, J. M.; Wondratschek, H. PSEUDO: a program for a pseudo-symmetry search. *J. Appl. Crystallogr.* **2001**, *34*, 783–784.

(51) Capillas, C.; Aroyo, M. I.; Perez-Mato, J. M. Methods for pseudosymmetry evaluation: a comparison between the atomic displacements and electron density approaches. *Z. Kristallogr. - Cryst. Mater.* **2005**, *220*, 691–699.

(52) Capillas, C.; Tasci, E. S.; de la Flor, G.; Orobengoa, D.; Perez-Mato, J. M.; Aroyo, M. I. A new computer tool at the Bilbao Crystallographic Server to detect and characterize pseudosymmetry. *Z. Kristallogr. - Cryst. Mater.* **2011**, *226*, 186–196.

(53) Bilbao Crystallographic Server, http://www.cryst.ehu.es/.

(54) Aroyo, M. I.; Perez-Mato, J. M.; Capillas, C.; Kroumova, E.; Ivantchev, S.; Madariaga, G.; Kirov, A.; Wondratschek, H. Bilbao Crystallographic Server: I. Databases and crystallographic computing programs. *Z. Kristallogr. - Cryst. Mater.* **2006**, *221*, 15–27.

(55) Aroyo, M. I.; Kirov, A.; Capillas, C.; Perez-Mato, J. M.; Wondratschek, H. Bilbao Crystallographic Server. II. Representations of crystallographic point groups and space groups. *Acta Crystallogr., Sect. A* **2006**, *62*, 115–128.

(56) Aroyo, M. I.; Perez-Mato, J. M.; Orobengoa, D.; E., T.; de la Flor, G.; Kirov, A. Crystallography online: Bilbao Crystallographic Server. *Bulg. Chem. Commun.* **2011**, *43*, 183–197.

(57) Monkhorst, H. J.; Pack, J. D. Special points for Brillouin-zone integrations. *Phys. Rev. B* **1976**, *13*, 5188–5192.

(58) Currao, A.; Curda, J.; Nesper, R. Kann man die Arten von Zintl-Anionen steuern? Variationen über das Thema Si^{2-} im System Sr/Mg/Si. *Z. Anorg. Allg. Chem.* **1996**, *622*, 85–94.

(59) Merlo, F.; Fornasini, M. CrB-type equiatomic compounds of europium, ytterbium and alkaline-earth metals with Si, Ge, Sn, Pb. *J. Less-Common Met.* **1967**, *13*, 603 – 610.

(60) Holleman, A. F.; Wiberg, N.; Wiberg, E. *Lehrbuch der Anorganischen Chemie*, 102nd ed.; de Gruyer, 2008.

(61) Baudler, M.; Glinka, K. Open-Chain Polyphosphorus Hydrides (Phosphines). *Chem. Rev.* **1994**, *94*, 1273–1297.

(62) Carlsohn, B. Zur Frage der Existenz eines festen Phosphorwasserstoffs $(PH)_x$. Dissertation, Universität zu Köln, 1976.

(63) Reyes, E. C.; Stalder, E. D.; Mensing, C.; Budnyk, S.; Nesper, R. Unexpected Magnetism in Alkaline Earth Monosilicides. *The Journal of Physical Chemistry C* **2011**, *115*, 1090–1095.

(64) Reyes, E. C.; Nesper, R. Electronic Structure and Properties of the Alkaline Earth Monosilicides. *The Journal of Physical Chemistry C* **2012**, *116*, 2536–2542.

(65) Kurylyshyn, I. M.; Fässler, T. F.; Fischer, A.; Hauf, C.; Eickerling, G.; Presnitz, M.; Scherer, W. Probing the Zintl-Klemm Concept: A Combined Experimental and Theoretical Charge Density Study of the Zintl Phase CaSi. *Angewandte Chemie International Edition* **2014**, *53*, 3029–3032.

(66) Maley, I. J.; Brown, D. H.; Ibberson, R. M.; Pulham, C. R. Solid-state structures of the covalent hydrides germane and stannane. *Acta Crystallogr., Sect. B* **2008**, *64*, 312–317.

(67) Puhakainen, K.; Benson, D.; Nyln, J.; Konar, S.; Stoyanov, E.; Leinenweber, K.; Hussermann, U. Hypervalent Octahedral SiH_6^{2-} Species from High-Pressure Synthesis. *Angew. Chem. Int. Ed.* **2012**, *51*, 3156–3160.

(68) Schiferl, D.; Barrett, C. S. The crystal structure of arsenic at 4.2, 78 and 299K. *J. Appl. Crystal.* **1969**, *2*, 30–36.

(69) Brown, A.; Rundqvist, S. Refinement of the crystal structure of black phosphorus. *Acta Crystal.* **1965**, *19*, 684–685.

(70) Nicol, A.; Vaughan, R. Proton chemical shift tensors of alkaline earth hydrides. *J. Chem. Phys.* **1978**, *69*, 5211–5213.

(71) Jehle, M.; Hoffmann, A.; Kohlmann, H.; Scherer, H.; Roehr, C. The 'sub' metallide oxide hydrides $Sr_{21}Si_2O_5H_{12+x}$ and $Ba_{21}M_2O_5H_{12+x}$ (M= Zn, Cd, Hg, In, Tl, Si, Ge, Sn, Pb, As, Sb, Bi). *J. Alloys Compd.* **2015**, *623*, 164–177.

(72) Frotscher, M.; Hölzel, M.; Albert, B. Crystal Structures of the Metal Diborides ReB_2, RuB_2, and OsB_2 from Neutron Powder Diffraction. *Z. Anorg. Allg. Chem.* **2010**, *636*, 1783–1786.

For Table of Contents Only

$_1^\infty[(HGe_6H)^{6-}]$

$_1^\infty[(SiH)^-]$
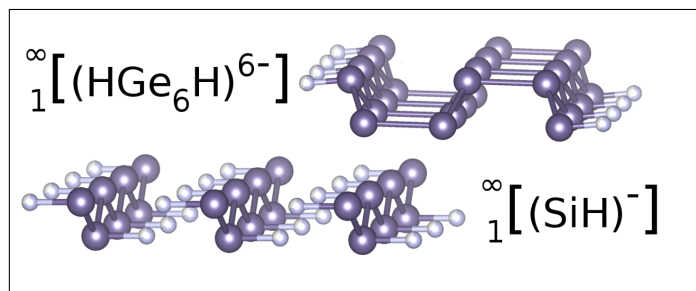
The hydrogenation of the Zintl phases BaSi, SrGe and BaSn leads to the formation of polyanionic hydride partial structures with covalent Tt-H (Tt = Si, Ge, Sn) bonds.